Seeded latex polymerizations: studies on the particle growth mechanism of latex particles

Show-An Chen and Song-Tai Lee
Chemical Engineering Department, National Tsing-Hua University, Hsinchu, Taiwan 30043, China
(Received 31 December 1990; accepted 23 May 1991)

In order to clarify the particle growth mechanism of latex particles, we performed a series of seeded styrene latex polymerizations using minor amounts of isoprene to tag the newly generated polymers. Morphological studies of microtomed particles are presented. It was found that the monomer distribution within the particle was rather uniform. If the particle is larger than a critical value ($\sim$0.15–0.20 μm), due to surface anchoring of the hydrophilic chain ends on the particle, the shell growth mechanism occurs. The polymerization takes place primarily in the shell region which is about the size of the end-to-end distance of the growing radicals ($\sim$0.01–0.04 μm). For small latex particles (particle diameter $< \sim$0.15 μm), a homogeneous reaction occurs inside the particles. Further evidence of the conversion data and molecular weight distributions also confirms the proposed shell growth mechanism.

(Keywords: latex polymerization; seeding; shell growth mechanism)

INTRODUCTION

Since Williams *et al.*[1,2] reported experimental evidence for the non-uniform 'core–shell theory' in styrene latex polymerizations, many controversial arguments about the theory have been presented[3–14]. Their consideration was based on the result of the constant polymerization rate well beyond the end of interval II (up to $\sim$60% conversion)[1]. They suggested that this result could be explained by a constant monomer concentration at the polymerization site in the particles, and proposed a core–shell theory by which the growing particle consists of a polymer-rich core and a monomer-rich shell. Later, they[2] gave morphological evidence of the core–shell morphology to support their theory. The core–shell theory, however, still had many unresolved conflicts of evidence[3–5]. Napper[3] pointed out that the diffusion rates of the monomer in the particles would not support the concept of such non-uniform swelling particles. Moreover, Gardon[4] pointed out that the much larger diffusive mean free path of the monomer molecules than the radius of the polymer particles would not favour the core–shell equilibrium theory. Gardon[4] also indicated that the results from the constant polymerization rate in Williams' work[1] can be attributed to the compensation of the decreasing monomer concentration by the increasing average number of free radicals per particle during interval III. The mechanism for the formation of core–shell morphology is still unknown[5].

Several years later, Vanderhoff[6] found experimental evidence of surface anchoring of hydrophilic sulphate chain ends on the particle surface for the growing radicals by conductometric titration. This result provided a possible explanation for the non-uniform particle morphology observed by Williams *et al.*[2]. Chern and Poehlein[7] further considered the Williams' core–shell morphology as a result of a non-uniform distribution of free radicals in the particle. Fisher *et al.*[8] used small-angle neutron scattering (SANS) to analyse the final latex particles (particle diameter, $D_p = 0.05$ μm) from the seeded latex polymerization of poly(methyl methacrylate); they also found that the latex particles had core–shell morphology. On the other hand, Goodwin *et al.*[9] also used SANS to analyse the monomer-swollen particles ($D_p = 0.42$ μm) of polystyrene and found that the particles remain homogeneous during the swelling process.

In systems of emulsifier-free latex polymerization, both Hearn *et al.*[10,11] and Chen *et al.*[12,13] found a bimodal molecular weight distribution (*MWD*) which was ascribed to two kinds of reaction loci of the particles. Chen and Chang[13] also found that the conversion curves were strongly influenced by the particle size via a series of seeded polymerizations. Besides, Chang and Chen[12] further proposed a 'diffusion-controlled core–shell model' and postulated a non-uniform morphology of the growing particles which consists of a nearly dry core (without monomer in the inner part of the particle) to explain the observed apparent linearity of $(\text{conversion})^{2/3}$ against time for conversions up to $\sim$40%. However, no direct evidence was provided to support the existence of the non-uniform particle morphology of dry core and wet shell during the post nucleation stage.

Recently, Chen *et al.*[14] proposed a 'shell growth mechanism' to explain the linearity of $(\text{conversion})^{2/3}$ against time in systems of emulsifier-free latex polymerizations. The shell growth mechanism is based on the idea that polymerization occurs mainly in the shell region ($\sim$0.01–0.04 μm), even though the monomer distribution in the particle is considered to be rather uniform. The reason for the occurrence of the shell growth

0032-3861/92/071437-08

mechanism is due to surface anchoring of the hydrophilic end groups and to the large size of the particles ($> \sim 0.15$–$0.20\ \mu m$). Since each growing radical has sulphate chain ends suspending on the particle surface[6], the growing end must locate within the shell with a thickness equal to its end-to-end distance. For large latex particles, a high average number of growing radicals ($\bar{n}$) will exist. The high $\bar{n}$ value then causes a termination of the growing radicals at lower molecular weight, which means that the growing radical chains have no chance to grow to a length long enough to arrive at the central region of the particles. However, no direct evidence was given to support the proposed shell growth mechanism.

This study aims to clarify the growth mechanism of the latex particles by performing a series of seeded styrene latex polymerizations. Morphological studies of microtomed particles provide direct evidence to support this mechanism. Conversion curves and *MWD*s are also found to be consistent with the shell growth mechanism.

EXPERIMENTAL

Materials

Styrene was used after purification by the usual method[15]. Water was freshly deionized. Acrylamide (AAm) and potassium persulphate (KPS) were recrystallized from benzene and deionized water before use, respectively. Sodium *p*-styrenesulphonate (NaSS) was used as received from Wako Co. Isoprene, sodium lauryl sulphate (SLS), 2,2′-azobisisobutyronitrile (AIBN) and tetrahydrofuran (THF) were used as received from Merck Co. The epoxy resin (Epon 812), its curing agent 2,4,6-dimethylaminomethyl phenol (DMP-30), the hardener dodecenyl succinic anhydride (DDSA), nadic methyl anhydride (NMA), and the staining agent osmium tetroxide (OsO_4), were used as received from Electron Microscopy Science Co.

Procedure

Latex polymerizations were carried out in a 500 ml four-neck reactor continuously purged with nitrogen. For run S2, a 1 l reactor was used to produce the seed latex. The reactor was equipped with a Teflon mixer, condenser and thermocouple with a rubber septum on one neck for taking samples. The agitation speed was 200 ± 20 rev min^{-1}.

To explore the dependence of the particle growth mechanism on particle size, we undertook seeded latex polymerizations as follows. Specific amounts of monomers (styrene and a trace amount of isoprene) were added to a seed latex. The mixture was agitated at 0°C for 24 h to allow the monomers to penetrate into the central region of the particles, and then heated to 70°C. Subsequently the initiator (KPS) was added to start the reaction at 70°C. For run H4, the initiator (AIBN) together with the monomers were added at the beginning of the swelling procedure. In the particles, isoprene should distribute uniformly and can copolymerize with styrene. Since the residual unsaturation in the isoprene units can be stained by OsO_4, isoprene was served to tag polymers generated in this period. The details for all the runs are listed in *Table 1*.

The particle diameter and morphology of the microtomed particles were determined by transmission electron microscopy (TEM). The microscopes used were H-600 from Hitachi Co. and JEOL 200 CX STEM from Japan Electron Optics Laboratory.

Specimens of microtomed particles for TEM examination were prepared in the following way. Dried

Table 1 Seeded latex polymerizations[a]

Run	Latex (g)	St (g)	KPS (g)	H_2O (g)	Isoprene (g)	AIBN (g)	Additives (g)	D_p[b] (μm)	Temp. (°C)	*Figure*
Seed latex										
S1		30	0.50	400			0.2(AAm)	0.51	70	*6c* and *d*
S2		100	1.00	800				0.92	70	*2a–d*
S3		20	0.40	400			0.4(SLS)	0.07	70	
S4		20	0.50	400			0.4(NaSS)	0.09	70	
Core–shell morphology										
C1	50(S1)	8	0.07	214	0.3			0.65	70	*1a–c*
C2	80(S2)	20	0.30	349	0.4			1.40	70	*1d–g*
C3	80(S2)	20	0.40	349	0.4			1.40	70	*7a–d*; *10*
Homogeneous morphology										
H1	100(S3)	40	0.30	310	0.5			0.13	65	*4a* and *b*; *12*
H2	100(S3)	40	0.40	310	0.5			0.13	65	*4c* and *d*
H3	100(S4)	5	0.05	181	0.1			0.11	70	*4e* and *f*
H4	50(S1)	4		138	0.2	0.008	0.1(SLS)	0.55	70	*3a–f*
Morphology from multi-feed (successive seeding) polymerization										
M1	100(H4)	5	0.05	95				0.71	70	*5a–d*
Miscellaneous										
V1		50	0.50	400				0.54	70	*6a* and *b*
V2	40(S2)	40	0.40	410	0.6			(c)	70	*12*

[a]St, styrene; KPS, potassium persulphate; AIBN, 2,2′-azobisisobutyronitrile; SLS, sodium lauryl sulphate; AAm, acrylamide; NaSS, sodium *p*-styrenesulphonate; D_p, particle diameter; Temp., temperature
[b]Monodisperse of the particle size distribution except for run V2
[c]Bimodal distribution of the particle size

latex particles (0.05 parts by weight) were mixed with the embedding resin (2 parts by weight) and then cured at 60°C for 2 days. The embedding resin consists of Epon 812, DDSA, NMA and DMP-30 (4.60/2.85/2.54/0.15 w/w). The cured mass was microtomed to give a thin slice (<0.09 μm), which was then transferred to a copper grid. The slice showed a silver to gray diffraction pattern, indicating a thickness of <0.09 μm. This visual method is normally used to estimate the thickness of slices from microtome sectioning. The whole assembly was exposed to the vapour from the mixture of OsO_4/water/acetone (2/49/49 w/w) at 25°C for 72 h. It was subsequently washed with water, vacuum dried and examined under the electron microscope.

For determination of the conversion curves, the samples withdrawn from the reactor were first exposed to air, quenched in an ice–water bath, and then vacuum-dried under room temperature. Although no inhibitor was added, it was found that addition of the inhibitor hydroquinone to the samples before drying provided no additional inhibition effect in the determination of conversion. Molecular weight distributions were measured using g.p.c. with dual detectors for comparison, an u.v. detector at a wavelength of 254 nm and a refractive index detector. The columns used were two Ultrastyragel columns (Waters Co.) in series having the regular molecular weight exclusion limit from 2×10^3 to 10^6. The flow rate of the carrier solvent (THF) was 1 ml min^{-1}.

RESULTS AND DISCUSSION

For all the reaction runs of series C, H and M listed in *Table 1*, the final latex particles of each run are spherical and have uniform size as shown in *Figures 1–8*. Thus, in each run, each particle was subjected to the same extent of reaction and the electron micrograph of any sectioned particle is representative. The sectioned particles are highly distorted and are larger than the original particles. This is due to swelling of the particles by absorption of the embedding resin into the particle during the sample preparation for TEM examination. Nevertheless, the contrast in the electron micrographs is developed so well that the characteristic morphology of the systems can be easily identified as shown in *Figures 1–5* and *7*.

Using the latices having D_p of 0.51 μm (obtained from run S1) and 0.92 μm (obtained from run S2) as the seeds, three runs of styrene latex polymerizations were carried out in the presence of a minor amount of isoprene (runs C1–C3). The resulting particles exhibit a core–shell morphology as shown in *Figures 1b*, *c* and *e–g*, respectively. The presence of a dark shell region indicates that only the shell region of the particles was stained, i.e. polymerization only occurred in this region. The shell thickness in these micrographs is greater than the theoretical value calculated from the amount of added monomer. This is also due to swelling of the particles by absorption of the embedding resin into the particle during sample preparation for TEM examination.

The dark ring of the core–shell morphology cannot be due to phase separation of polystyrene and styrene–isoprene copolymer within the particle, because the dark region in the micrograph of the stained film cast from toluene solution (*Figures 2a* and *b*) is quite different from those of the core–shell morphology shown in *Figures 1e–g*. In addition, the dark ring cannot be due to higher sulphate contents in the region close to the surface, since the micrograph of the OsO_4-stained sectioned seed particle from run S2 shows no dark ring (*Figures 2c* and *d*).

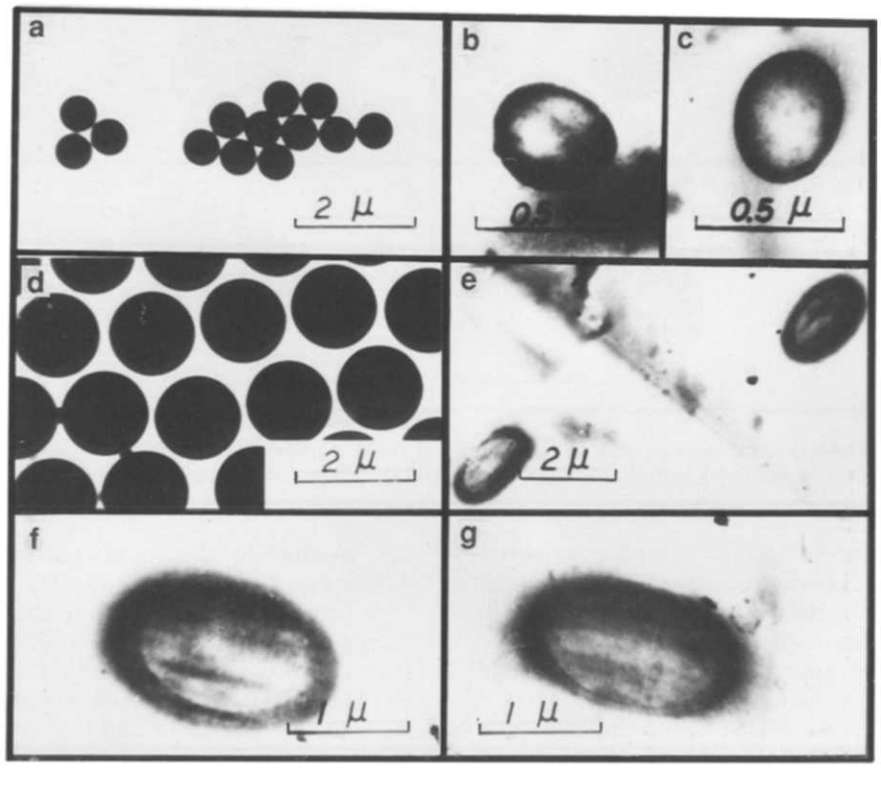

Figure 1 Transmission electron micrographs of the core–shell morphology for large particles, OsO_4 stained: (a) particles of run C1; (b, c) microtomed sections for particles of run C1; (d) particles of run C2; (e–g) microtomed sections for particles of run C2

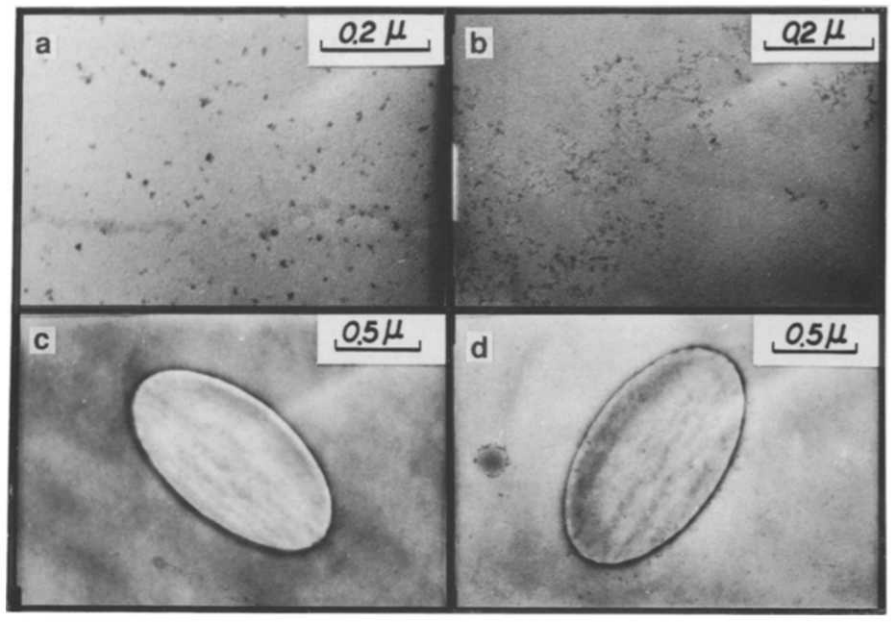

Figure 2 Transmission electron micrographs of run S2, OsO_4 stained: (a, b) solution cast film; (c, d) microtomed sections of the particles

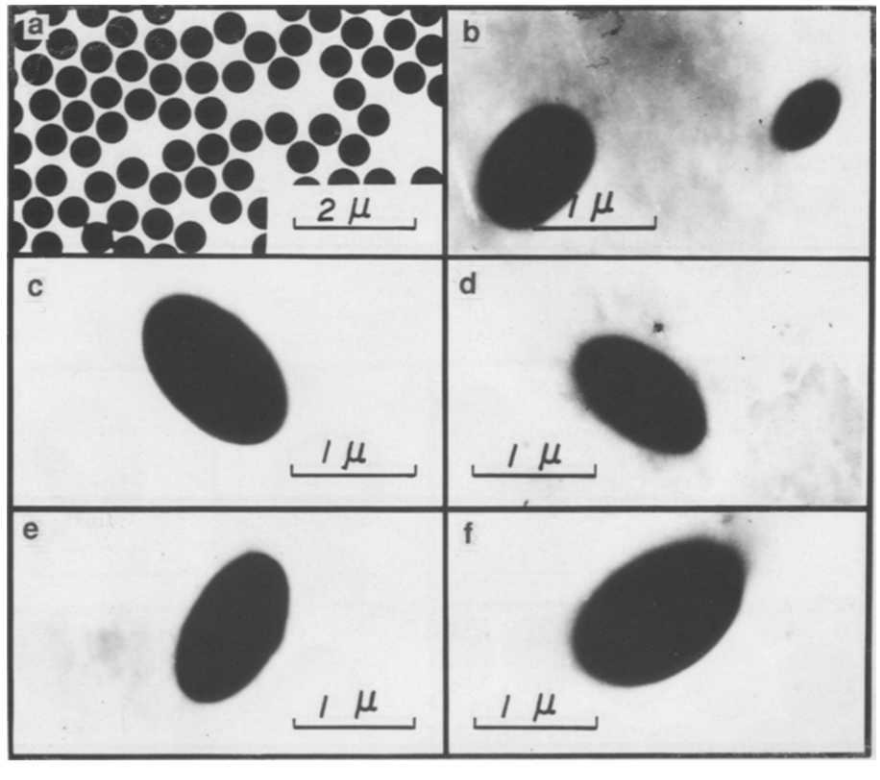

Figure 3 Transmission electron micrographs of the homogeneous morphology with AIBN, OsO_4 stained: (a) particles of run H4; (b–f) microtomed sections for particles of run H4

To elucidate the dominating factors for the formation of the core–shell morphology, we also used the oil soluble initiator AIBN instead of the water soluble initiator KPS, in reaction run H4. As monomer is distributed everywhere in its seed (S1), the introduction of AIBN should allow styrene to react with isoprene throughout the particle. The microtomed particles of H4 show uniform morphology as shown in *Figures 3b–f*. This further indicates that the core–shell morphology is not due to non-uniform swelling or a monomer diffusion-controlled mechanism. In addition, this observation also indicates that swelling for 24 h is sufficient for the monomers to diffuse into the centre of the latex particle.

In order to confirm that the shell growth mechanism should not occur for small seed, the D_p of the seed is reduced to 0.07 and 0.09 μm (obtained from runs S3 and S4); particles of the resulting latices H1, H2 and H3 have D_p values of 0.13, 0.13 and 0.11 μm, respectively. Their microtomed particles exhibit uniform morphology as shown in *Figures 4b, d* and *f*, indicating that the polymerization occurred uniformly within the small particles.

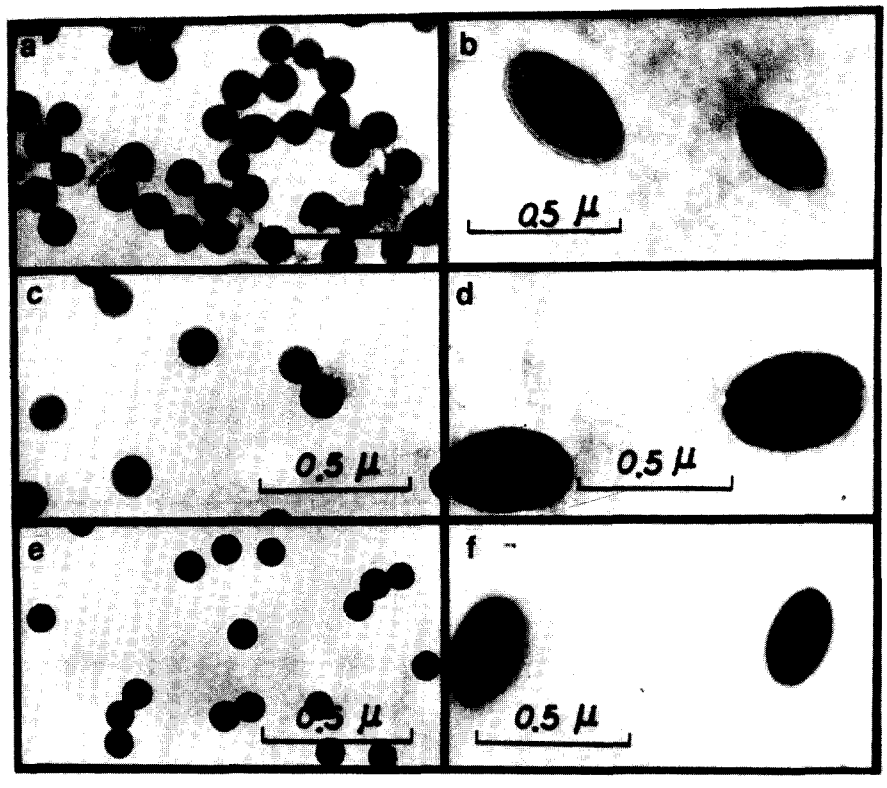

Figure 4 Transmission electron micrographs of the homogeneous morphology for small particles, OsO_4 stained: (a) particles of run H1; (b) microtomed sections for particles of run H1; (c) particles of run H2; (d) microtomed sections for particles of run H2; (e) particles of run H3; (f) microtomed sections for particles of run H3

The above results confirm that the shell growth mechanism occurs only as the growth particles have greater diameters ($> \sim 0.15$–$0.2\ \mu m$). The reason for this is that the growing radical has sulphate chain ends suspending on the particle surface, thus the growing ends must locate within the shell region having a thickness equal to the end-to-end distance of the growing polymeric radicals[14]. As the particle size is small ($< \sim 0.15\ \mu m$), it is highly improbable to have more than one radical in the particle during radical propagation; and the growing end of the radical chain is able to reach all locations within the particle. Consequently, the reaction follows the 0–1 system of the Smith–Ewart case II and generates high molecular weight polymers in small latex particles.

Another experiment for emphasizing the presence of the white shell is as follows. Using the latex from run H4 as the seed, styrene latex polymerization without addition of isoprene was carried out (run M1). The seed particle of run H4 has uniformly dispersed polystyrene chains tagged with isoprene units due to the use of AIBN, and thus has a homogeneous morphology as shown in *Figures 3b–f*. The resulting particle has a clear morphology of a dark core with a white shell as shown in *Figures 5b–d*. The sequence of white and dark regions is opposite to that of *Figures 1b*, *c* and *e–g*.

It was suggested by Williams and co-workers[1,2] that the core–shell morphology was developed due to non-uniform swelling of latex particles after equilibrium absorption of the monomer, the core being dry and the shell being monomer-rich. At first glance, it seems that the SANS data of Fisher *et al.*[8] would also support the hypothesis of non-uniform swelling. However, the emulsifiers (Triton-X-100 and Triton 770) used by Williams *et al.* and Fisher *et al.* can create strong chain transfer reactions and may develop a core–shell morphology of the final particles[5]. It is worth noting that the non-uniform core–shell morphology cannot be interpreted as exclusive evidence for non-uniform swelling of the monomer-swollen particles. On the other hand, the SANS data of Goodwin *et al.*[9] supported the uniform swelling mechanism of the monomer-swollen particles. In our emulsifier-free latex polymerizations, the morphology of the void particles (*Figures 6a* and *c*), resulting from dynamic vacuum pumping of the latex at an earlier stage of polymerization, indicates that the monomer distribution in the particle should be rather uniform. In addition, the presence of homogeneous morphology in *Figures 3* and *4* provides further evidence of uniform swelling. Furthermore, the dark core in *Figures 5b–d*, which is essentially the particle of run H4 as shown in *Figure 3*, provides a good contrast with the morphology of uniform swelling in *Figures 3* and *4*.

It may also be suggested that the core–shell morphology was developed exclusively due to a diffusion-controlled formation in the final 10–20% conversion period of the latex particles. To elucidate which is the dominating factor in the core–shell morphology in run C3, we present the morphology of the sectioned particle at 83% conversion of the added monomers in *Figure 7b* and those at 33% conversion in *Figures 7c* and *d*. The core–shell morphology shown in *Figures 7c* and *d* for the 33% conversion particles also gave direct evidence for the validity of the shell growth mechanism. The core–shell morphology is the result of surface anchoring of the growing radicals but not of diffusion control of the

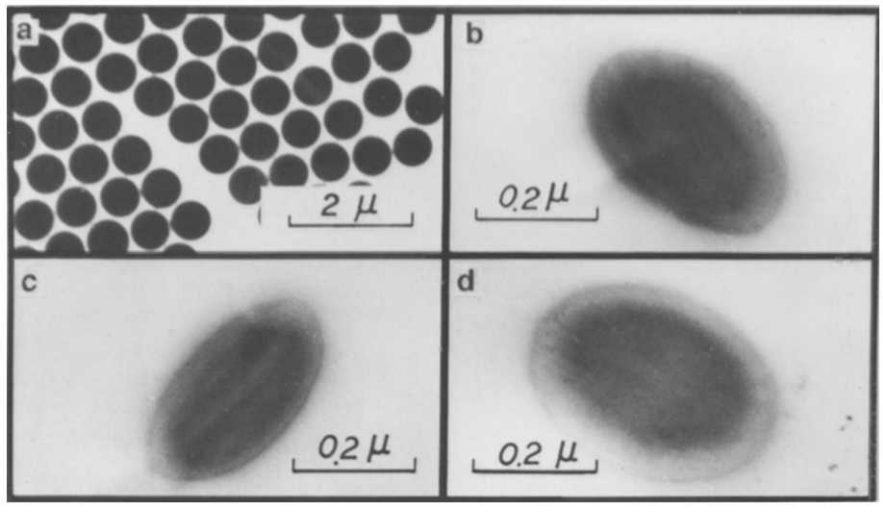

Figure 5 Transmission electron micrographs of the core–shell morphology from multi-feed, OsO_4 stained: (a) particles of run M1; (b–d) microtomed sections for particles of run M1

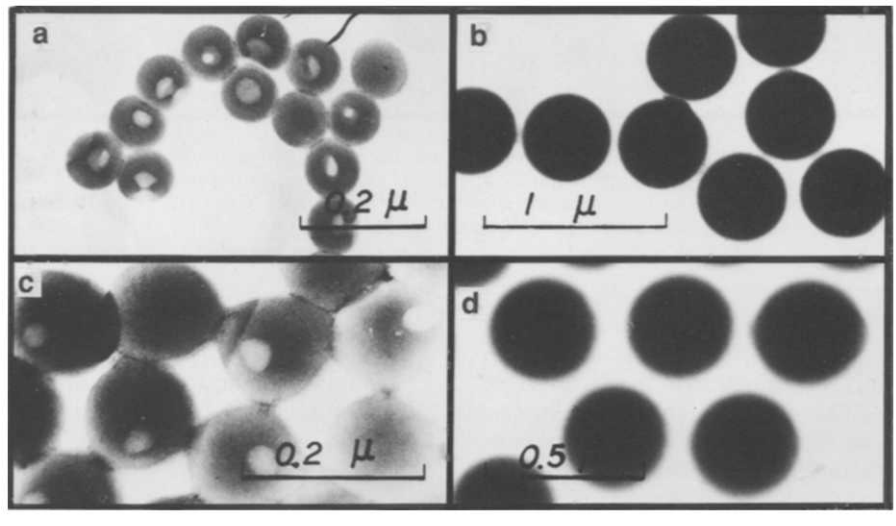

Figure 6 Electron micrographs of the particles of reaction run V1: (a) 2% conversion, (b) 80% conversion; and those of reaction run S1: (c) 2.7% conversion, (d) 90.3% conversion

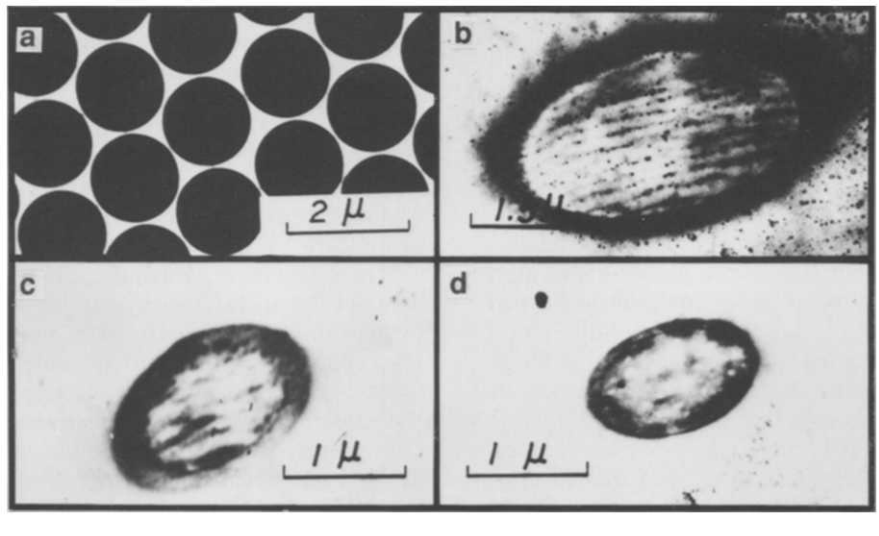

Figure 7 Transmission electron micrographs of the core–shell morphology for particles of run C3 at different conversions of added monomers, OsO_4 stained: (a) particles of run C3; (b) microtomed sections for particles of run C3 at 83% conversion; (c, d) microtomed sections for particles of run C3 at 33% conversion. The conversion curve is shown in *Figure 9*

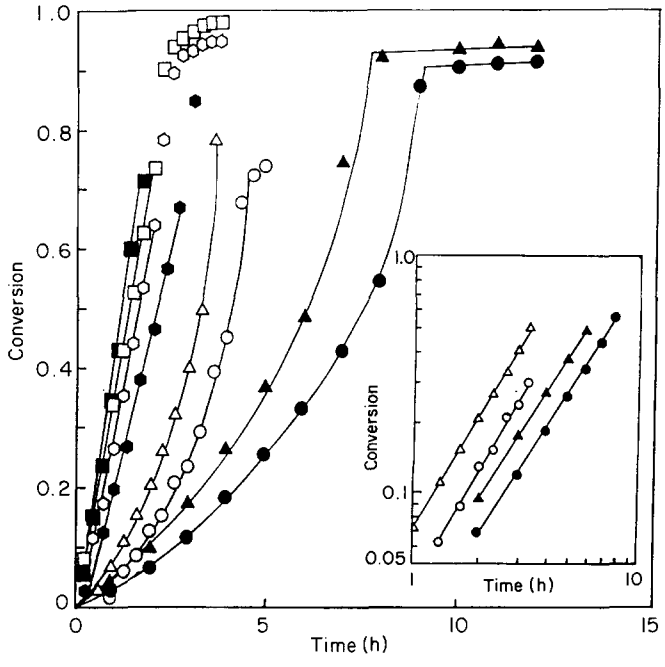

Figure 8 Conversion curves of the added monomers for seeded latex polymerizations (D_p of the seed is shown in parentheses): (□) (0.07 μm) H2; (○) (0.07 μm) H1; (△) (0.92 μm) C3; (○) (0.92 μm) C2. Also, conversion curves of emulsifier-free latex polymerizations (the final D_p is shown in parentheses): (■) (0.15 μm) NaUI[15]; (○) (0.15 μm) NaSS[16]; (▲) (0.51 μm) S1; (●) (0.54 μm) V1. The inset shows a log/log plot in which the slopes for runs C3, C2, S1 and V1 are 1.58, 1.68, 1.45 and 1.48, respectively

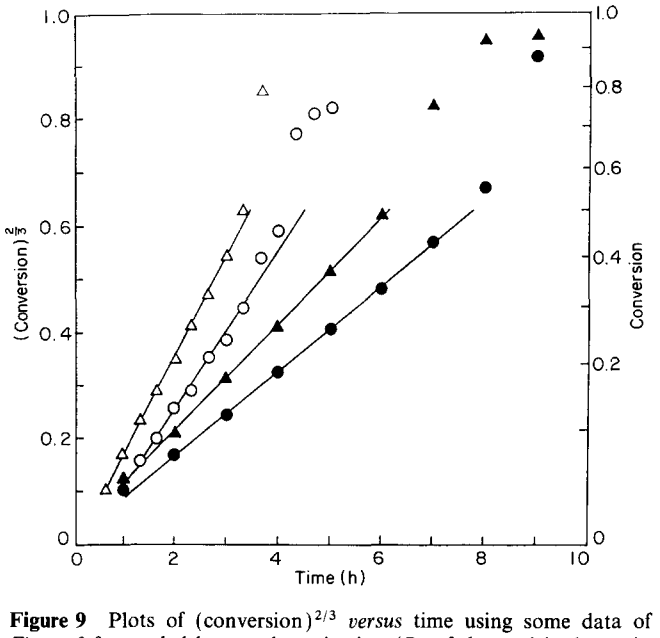

Figure 9 Plots of (conversion)$^{2/3}$ *versus* time using some data of *Figure 8* for seeded latex polymerization (D_p of the seed is shown in parentheses): (△) (0.92 μm) C3; (○) (0.92 μm) C2. Also, emulsifier-free latex polymerizations (the final D_p is shown in parentheses): (▲) (0.51 μm) S1; (●) (0.54 μm) V1

monomers. As a result, the morphologies of core–shell and multi-shell shown above result solely from the shell growth mechanism.

According to the shell growth mechanism, equation (1) should be applied to systems containing large particles ($> \sim 0.15$ μm)[5,12,14]:

$$m^{2/3} - m_0^{2/3} = K't \qquad (1)$$

where m and m_0 are conversions at time t and t_0 and K' is a constant. Therefore, if the shell growth mechanism can be applied to the system, the characteristic slope of the log/log plot of conversion *versus* time should be equal to 1.5 in the period of particle growth. In an emulsifier-free system with large D_p, each conversion curve is concave upwards (*Figure 8*), the log/log plot of conversion *versus* time gives a straight line with slope ranging from 1.45 to 1.48 in the range of 10–50% conversion (inset in *Figure 8*). In seeded latex polymerizations with small seed latex ($D_p < 0.15$ μm), the conversion curve is linear before ~60% conversion (*Figure 8*). On the other hand, in those with large seed latex ($D_p > 0.15$ μm), each conversion curve is concave upwards, the log/log plot of conversion *versus* time gives a straight line with slope ranging from 1.58 to 1.68 in the range of 10–50% conversions (inset in *Figure 8*). Consequently, the plot of (conversion)$^{2/3}$ *versus* time for each case referred to large D_p also gives a straight line, which is the characteristic feature of the shell growth mechanism, in the same conversion range without appreciable errors (*Figure 9*). According to the discussions above, the shell growth mechanism can be applied to systems of seeded as well as emulsifier-free latex polymerizations. Because radicals in the particle have to build up from zero to the equilibrium value, the seed particles contain no radicals and obviously there is an unsteady-state situation in the beginning of the reaction[5]. Therefore, the linearity of (conversion)$^{2/3}$ against time does not hold at the beginning of the seeded latex polymerization.

The major *MWD* of polymers newly generated for run C3 (with $D_p = 0.92$ μm) is $\sim 10^4$–10^5, while that of run H1 (with $D_p = 0.07$ μm) is $\sim 10^5$–10^6 (*Figures 10* and *11*). For polystyrene at the θ condition[17], the root mean square end-to-end distance $(\langle \bar{r}^2 \rangle)^{1/2}$ calculated from the equation $(\langle \bar{r}^2 \rangle / M_w)^{1/2} = 0.71$ Å is 710 Å for $\bar{M}_w = 10^6$ and 225 Å for $\bar{M}_w = 10^5$. The former molecular weight is

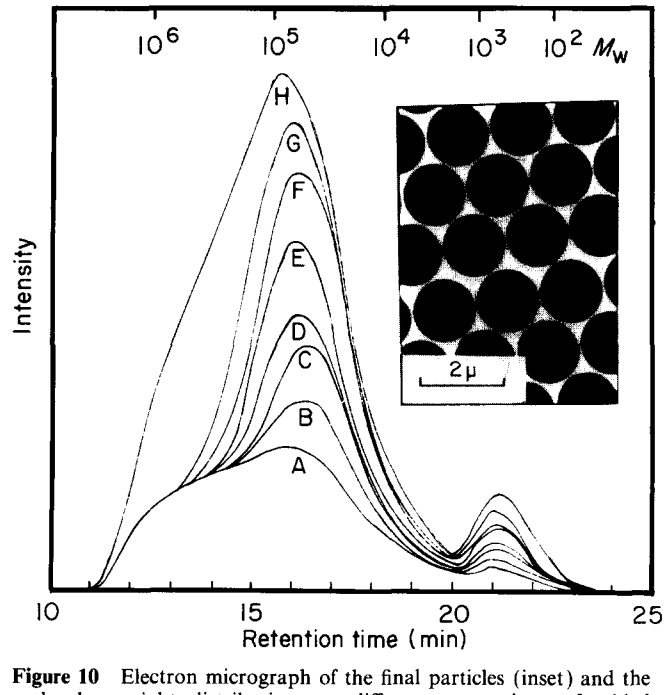

Figure 10 Electron micrograph of the final particles (inset) and the molecular weight distributions at different conversions of added monomers for run C3: seed S2 with $D_p = 0.92$ μm (A), 3.3% (B), 11.3% (C), 15.7% (D), 26.6% (E), 40.3% (F), 49.8% (G), 78.8% (H). The area below each curve is about proportional to the weight fraction of the polymer in the reactor at the sampling time

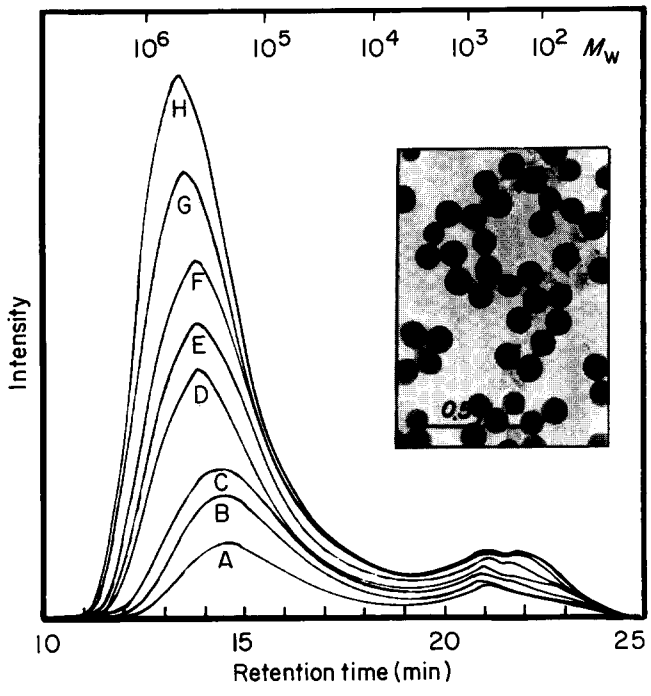

Figure 11 Electron micrograph of the final particles (inset) and the molecular weight distributions at different conversions of added monomers for run H1: seed S3 with $D_p = 0.07\ \mu m$ (A), 8.4% (B), 15.9% (C), 24.6% (D), 43.3% (E), 53.4% (F), 63.0% (G), 74.0% (H). The area below each curve is about proportional to the weight fraction of the polymer in the reactor at the sampling time

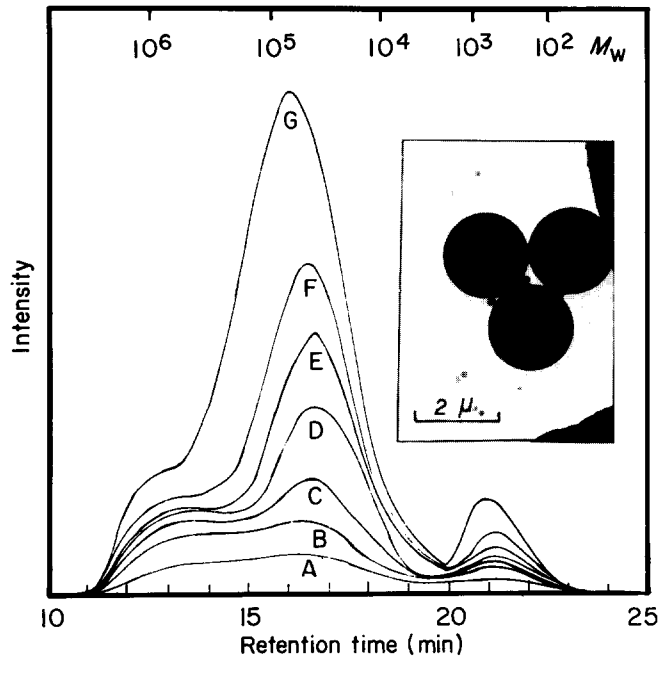

Figure 12 Electron micrograph of the final particles (inset) and the molecular weight distributions at different conversions of added monomers for run V2: seed S2 (A), 9.9% (B), 20.0% (C), 30.1% (D), 40.1% (E), 53.8% (F), 90.1% (G). The area below each curve is about proportional to the weight fraction of the polymer in the reactor at the sampling time

typical for conventional latex polymerization[18] (Smith–Ewart case II), while the latter value is typical for the shell growth period. Such a molecular weight value in the growth period must be due to the growing radicals having a higher chance to terminate with the other entering radicals or the other growing radicals co-existing in the reactive region of the particle. From the above analysis, it is clear that the shell growth mechanism is consistent with the conversion and *MWD* data. If a second nucleation takes place in the reactor, there will be at least two kinds of reaction loci in the reactor. As shown in *Figure 12*, both the higher molecular weight peak ($\sim 10^6$) and the medium peak ($\sim 10^4$–10^5) increase in height as the reaction proceeds. The former is due to the polymer generated in the small particles while the latter is generated by the large particles. Thus the shape of the conversion curve depends on the ratio of the number of small particles to large ones.

CONCLUSIONS

Even though the monomer distribution in the particle is rather uniform, the growth of latex particles follows the shell growth mechanism. This mechanism was considered to result from the anchoring of hydrophilic chain ends of the growing radicals on the particle surface and from the high average number of radicals per particle.

ACKNOWLEDGEMENT

The authors wish to thank the National Science Council for financial aid through the project, Studies on Emulsion Polymer Science, NSC 79-0405-E007-05.

REFERENCES

1 Grancio, M. R. and Williams, D. J. *J. Polym. Sci. A1* 1970, **8**, 2617
2 Keusch, P. and Williams, D. J. *J. Polym. Sci., Polym. Chem. Edn.* 1973, **11**, 143
3 Napper, D. H. *J. Polym. Sci. A1* 1971, **9**, 2089
4 Gardon, J. L. *J. Polym. Sci., Polym. Chem. Edn.* 1973, **11**, 241; 1974, **12**, 2133
5 Ugelstad, J. and Hansen, F. K. *Rubber Chem. Technol.* 1976, **49**, 536
6 Vanderhoff, J. W. in 'Characterization of Metal and Polymer Surfaces' (Ed. L. H. Lee), Academic Press, 1977, p. 365
7 Chern, C. S. and Poehlein, G. W. *J. Polym. Sci., Polym. Chem. Edn.* 1987, **25**, 617
8 Fisher, L. W., Melpolder, S. M., O'Reilly, J. M., Ramakrishnan, V. and Wignall, G. W. *J. Coll. Int. Sci.* 1988, **123**, 24
9 Goodwin, J. W., Ottewill, R. H., Harris, N. M. and Tabony, J. *J. Coll. Int. Sci.* 1980, **78** (1), 253
10 Goodall, A. R., Wilkinson, M. C. and Hearn, J. *J. Polym. Sci., Polym. Chem. Edn.* 1977, **15**, 2193
11 Hearn, J., Wilkinson, M. C., Goodall, A. R. and Chainey, M. *J. Polym. Sci., Polym. Chem. Edn.* 1985, **23**, 1869
12 Chang, H.-S. and Chen, S.-A. *J. Polym. Sci., Polym. Chem. Edn.* 1988, **26**, 1207
13 Chen, S.-A. and Chang, H.-S. *J. Polym. Sci., Polym. Chem. Edn.* in press
14 Chen, S.-A., Lee, S.-T. and Lee, S.-J. Paper presented at the 2nd International Symposium on Copolymerization and Copolymers in Dispersed Media, Lyon, France, April 1989; *Makromol. Chem. Macromol. Symp.* 1990, **35/36**, 349
15 Chen, S.-A. and Chang, H.-S. *J. Polym. Sci., Polym. Chem. Edn.* 1985, **23**, 2615
16 Juang, M. S. and Krieger, I. M. *J. Polym. Sci., Polym. Chem. Edn.* 1976, **14**, 2089
17 Flory, P. J. (Ed.) 'Principles of Polymer Chemistry,' Cornell University Press, Ithaca, 1953, p. 618
18 Gardon, J. L. in 'Polymerization Process' (Eds C. E. Schildknecht and I. Skeist), John Wiley, New York, 1977, p. 143